JPET Fast Forward. Published on September 1, 2017 as DOI: 10.1124/jpet.117.243097
This article has not been copyedited and formatted. The final version may differ from this version.

A model of the block of Kv4.2 ionic currents by 4-aminopyridine

Steven J. Kehl

Department of Cellular and Physiological Sciences, University of British Columbia, Vancouver, British Columbia, Canada

JPET Fast Forward. Published on September 1, 2017 as DOI: 10.1124/jpet.117.243097
This article has not been copyedited and formatted. The final version may differ from this version.

Running Title: 4AP block of Kv4.2

Address for reprint requests and other correspondence: S. J. Kehl, Dept. of Cellular and Physiological Sciences, Univ. of British Columbia, 2350 Health Sciences Mall, Vancouver, BC, Canada V6T 1Z3 (phone: 604-822-2185; e-mail: skehl@mail.ubc.ca)

Text pages: 26

Tables: 2

Figures: 7

References: 33

Abstract: 212 words

Introduction: 759 words

Discussion: 1518 words

Abrreviations:

4AP, 4-aminopyridine; CSI, closed state inactivation; GFL, giant fibre lobe; I_{to}, transient outward current; k_{on}, association rate constant; k_{off}, unbinding rate constant; Kv, voltage-gated potassium; QA, quaternary ammonium; SGA, squid giant axon; *Sh*IR, fast inactivation removed *Shaker* K^+ channel; $\tau_{unblock,}$ time constant for unblock; $\tau_{block,}$ time constant for block; TEA^+, tetraethylammonium ion; V_h, holding potential; V_{half}, voltage for half-maximal effect; *s*, slope factor

Recommended Section: Cellular and Molecular

JPET Fast Forward. Published on September 1, 2017 as DOI: 10.1124/jpet.117.243097
This article has not been copyedited and formatted. The final version may differ from this version.

Abstract

Voltage clamp recordings of macroscopic currents were made from rat Kv4.2 channels expressed in HEK293 cells. The main goals of the study were to quantify the concentration-, time- and voltage dependence of the block and to generate a state model that replicated the features of the block. When applied either externally or internally, the block of Kv4.2 currents by 4-aminopyridine (4AP) occurs at the holding potential (-80 mV), is affected by the stimulus frequency and is relieved by membrane depolarization. The K_d for the tonic block at -80 mV was 0.9 ± 0.07 mM and was consistent with 1:1 binding. Relief of block during a step to 50 mV was well-fitted by a single exponential with a time constant of ~40 ms. At -80 mV the association rate constant was 0.08 mM^{-1} s^{-1} and the off-rate was 0.08 s^{-1}. The state model replicates the features of the experimental data reasonably well by assuming that 4AP binds only to closed states, that 4AP binding and inactivation are mutually exclusive processes and that the activation of closed-bound channels is the same as for closed channels. Since the open channel has a very low or no affinity for 4AP, channel opening promotes the unbinding of 4AP which accounts for the reverse use-dependence of the block.

Introduction

Investigations of the mechanisms by which organic compounds affect ionic and gating currents mediated by voltage-gated channels have played an important role in developing our understanding of the molecular structure of ion channels. In the context of voltage-gated K^+ (K_v) channels, the seminal studies by Armstrong (1971) of the block of delayed rectifier K^+ channels of the squid giant axon (SGA) by quaternary ammonium (QA) compounds, such as tetraethylammonium ion (TEA^+), provided insights into the topology of the permeation pathway as well as the location and movement of the activation gate. Aminopyridines comprise another group of compounds that have been useful tools in the characterization of Kv channels. For example, 4-aminopyridine (4AP) was first reported to block axonal delayed rectifier currents from several invertebrate and vertebrate species (Yeh et al., 1976b; Kirsch and Narahashi, 1983) and more recently shown to block currents mediated by the fast inactivation-removed *Shaker* (*Sh*IR) channel (Castle et al., 1994a; McCormack et al., 1994), which is the *Drosophila* homologue of the Kv1 channel subfamily.

It has been proposed for *Shaker* channels (Armstrong and Loboda, 2001) that both TEA^+ and 4AP have a site of action in the inner vestibule of the pore (Armstrong, 1997) that is nominally equivalent to the central cavity identified in the crystal structure of the KcsA channel (Doyle et al., 1998). For both compounds the experimental data are consistent with the view that the access of internal 4AP (Kirsch and Drewe, 1993; McCormack et al., 1994) to a binding site in the central cavity is contingent on opening of the activation gate that otherwise prevents movement of compounds from the cytoplasmic compartment into the central cavity, and *vice versa* in the case of unbinding. A consequence of this strict coupling of binding to channel opening is that the block is use-dependent, meaning that membrane depolarization is required to initiate the block. The primary distinction between TEA^+ and 4AP is the outcome of binding in the central cavity. In the case of TEA^+, which is approximately the size of a hydrated K^+ ion, the inhibition of current comes about by a physical plugging of the permeation pathway. In the case of 4AP, which is smaller than TEA^+, binding in the central cavity of the *Shaker* channel is proposed to strongly bias the opening/closing transitions toward the closed state, thus decreasing the open probability (P_o). The latter effect is associated with no or minimal alteration of the kinetics or

JPET Fast Forward. Published on September 1, 2017 as DOI: 10.1124/jpet.117.243097
This article has not been copyedited and formatted. The final version may differ from this version.

voltage dependence of voltage sensor activation (McCormack et al., 1994; Loboda and Armstrong, 2001).

Fast-activating, fast-inactivating K^+ current, which is identified as I_{to} in cardiac myocytes and as I_A in central neurons, and which is mediated by Kv4 (*Shal*) channels (Fiset et al., 1997), is also blocked by 4AP. As first noted in the study by Thompson (1977), the properties of the block of I_A in molluscan central neurons showed some similarities to its block of the SGA delayed rectifier (Yeh et al., 1976a). Thus, 4AP block increases with hyperpolarization, is use-dependent and can be removed by depolarization. The block of I_{to} in ventricular myocytes (Campbell et al., 1993; Castle and Slawsky, 1993), of the transient K^+ current ($I_{K(f)}$) in pituitary melanotrophs (Kehl, 1990) and of Kv4.2 channels in a heterologous expression system (Tseng et al., 1996; Yeola and Snyders, 1997) suggested that 4AP binding and inactivation were mutually exclusive events, that is to say inactivation was prevented in 4AP-bound channels and 4AP binding was prevented by inactivation. Additionally, binding of 4AP occurred exclusively to one or more closed states which gives rise to the phenomenon of "reverse use-dependence" (Tseng et al., 1996) and distinguishes the 4AP block of transient K^+ currents from the block of *Shaker* channels.

To address the issue of the mechanism of action of 4AP in fast transient K^+ channels this study set two goals. The first was to describe the inhibition by 4AP of Kv4.2 channels expressed in HEK293 cells and to quantify the concentration-, time- and voltage dependence of the block. The second goal was to use the quantitative measures gleaned from the experimental data to constrain a numerical model of the actions of 4AP. The proposed model replicates the features of the experimental data reasonably well by assuming that 4AP binds to closed states, that 4AP binding and inactivation are mutually exclusive processes and that the activation of closed-bound channels is the same as for closed channels. By virtue of a low or no affinity of the open channel for 4AP, channel opening promotes the unbinding of 4AP which accounts for the reverse use-dependence of the block.

Methods

Cell preparation

JPET Fast Forward. Published on September 1, 2017 as DOI: 10.1124/jpet.117.243097
This article has not been copyedited and formatted. The final version may differ from this version.

Currents were recorded from rat Kv4.2 channels stably expressed in a human embryonic kidney cell line (HEK293; American Type Culture Collection, Rockville, MD, USA). Cells were passaged using trypsin-EDTA and maintained in minimum essential medium (MEM) supplemented with 10% fetal bovine serum, 1% penicillin-streptomycin and 0.5 mg ml^{-1} geneticin at 37ºC in an atmosphere of 5% CO_2 in air. All tissue culture supplies were obtained from Invitrogen (Burlington, ON, Canada).

Recording solutions

Unless otherwise stated, the standard bath solution contained (in mM): 140 NaCl, 3.5 KCl, 2 $CaCl_2$, 1 $MgCl_2$, 5 glucose, and 10 HEPES; the pH was adjusted with NaOH to 7.4 at room temperature. A stock solution of 4AP for bath application was prepared by dissolving 4-aminopyridine (Aldrich, ≥ 99%) in standard bath solution and then titrating to pH 7.4 with HCl. The patch pipette solution contained (in mM): 130 KCl, 4.75 $CaCl_2$ (*p*Ca = 7.3), 1.38 $MgCl_2$, 10 EGTA, 10 HEPES and was adjusted to pH 7.4 with KOH. For experiments assessing the effects of its internal application a 20 mM stock solution of 4AP was prepared in the patch pipette solution and then titrated to pH 7.4 with HCl. Chemicals were obtained from the Sigma Aldrich Chemical Company (Mississauga, ON, Canada).

In an experiment, a section of glass coverslip to which stably transfected HEK293 cells had adhered was placed in a recording chamber (0.5 ml volume). During an experiment the chamber was perfused with standard bath solution at a rate of 1-2 ml min^{-1}. External 4AP was applied using a fast-application pipette positioned within 100 µm of the test cell and rapid change of the pipette solution perfusing a test cell was digitally controlled (Cheng et al., 2010).

Electrophysiological procedures

Whole-cell currents were recorded at room temperature (20 - 25ºC) using an EPC-8 patch clamp amplifier connected to a computer via an ITC-18 digital interface (HEKA Electronik, Germany). Patch electrodes were made from thin-walled borosilicate glass (World Precision Instruments, Sarasota, FL) and had resistances of 1.0 - 1.5 MΩ measured in the recording chamber with the standard internal and external solutions. Voltage clamp commands were generated using HEKA PatchMaster software. Circuitry of the EPC-8 amplifier was used to compensate the membrane capacitance and at least 80% of the series resistance. Leak subtraction was not used. Current

signals were filtered at 3 kHz (−3dB, 8 pole Bessel filter) and digitised (16 bit resolution) at a sampling interval of 25-50 μs. Voltages were corrected for liquid junction potentials. The holding potential (V_h) was normally -80 mV and the test pulse potential was usually 50 mV. There was no compensation for the contribution of the endogenous, slowly-inactivating, delayed rectifier-type current expressed in HEK293 cells. In non-transfected cells in standard bath solution the endogenous K^+ current at 50 mV typically ranges from 0.4 to 1.4 nA.

As reported previously (Kehl et al., 2013), control Kv4.2 currents had biophysical properties (not shown) that quite closely matched those reported for rat Kv4.2 channels expressed in *Xenopus* oocytes (Tseng et al., 1996) and wild type human Kv4.2 channels expressed in HEK293 cells (Bahring et al., 2001). The midpoint of the steady-state availability curve was -59.3 ± 0.3 mV and the slope factor was 5.4 ± 0.2 mV (n = 9). Recovery from inactivation at -80 mV following a 300 ms step to 50 mV was monoexponential and had a time constant of 330 ± 14 ms (n = 15).

Data analysis

Data are presented as the mean ± the standard error of the mean, except for the values derived from non-linear least-squares fitting routines (Igor Pro 7, Wavemetrics, OR), which are expressed as the mean ± the standard deviation. The value for n represents the number of cells examined. The level for statistical significance was $P < 0.05$.

Concentration-response data were fitted to the Hill equation:

$$y = base + \frac{1 - base}{1 + \left\{\frac{[4AP]}{K_d}\right\}^h} \qquad (Eqn.\,1),$$

where y is the normalized peak current evoked at a given concentration of 4AP, *base* is the lower asymptote, K_d is the apparent equilibrium dissociation constant and h is the Hill coefficient.

Exponential relaxations were fitted either to a monoexponential,

$$y(t) = A_0 + A_1 \exp\left(-\frac{t}{\tau_1}\right) \qquad (Eqn.\,2)$$

or a biexponential function,

JPET Fast Forward. Published on September 1, 2017 as DOI: 10.1124/jpet.117.243097
This article has not been copyedited and formatted. The final version may differ from this version.

$$y(t) = A_0 + A_1 \exp\left(-\frac{t}{\tau_1}\right) + A_2 \exp\left(-\frac{t}{\tau_2}\right) \qquad (Eqn. 3),$$

where *y* is the current as a function of time (*t*), A_0 is the steady-state current, and A_1 and A_2 represent the proportion of the current fitted by an exponential with a time constant of τ_1 and τ_2, respectively.

Biphasic exponential relaxations, such as are observed in the time course of the recovery from inactivation and the onset of block (Fig. 4), were fitted using

$$y(t) = A_0 + A_1\left(1 - exp\left(-\frac{t}{\tau_1}\right)\right) + A_2 \exp\left(-\frac{t}{\tau_2}\right) \qquad (Eqn. 4),$$

where A_1 and A_2 represent the amplitudes of the rising and decaying components of the current, respectively.

For the analysis of the effect of a conditioning or pre-pulse potential on the block by 4AP (Fig. 6), peak test current amplitudes were normalized using

$$y = \frac{I_{max} - I_{test}}{I_{max} - I_{min}} \qquad (Eqn. 5),$$

where *y* is the relative block, I_{max} is the maximal peak current following a conditioning voltage of -30 mV, I_{test} is the peak test current following a given conditioning voltage and I_{min} is the peak test current following a conditioning voltage of -80 mV. Curves relating the relative block as a function of the conditioning voltage (V) were fitted to the Boltzmann equation,

$$relative\ block\ (V) = \frac{1}{1+\exp\left(\frac{V_{half} - V}{s}\right)} \qquad (Eqn.\ 6),$$

where V_{half} is the potential at which the block is half-maximal and *s*, the slope factor, indicates the steepness of the change of relative block (i.e., limiting slope of *e*-fold change per *s* mV).

Numerical Modelling

Macroscopic Kv4.2 currents were simulated and analyzed in Igor Pro 7 using built-in and user-generated functions and procedures. State occupancies as a function of time and voltage were calculated, as outlined by Colquhoun and Hawkes (2011), from the spectral expansion of the Q-matrix generated from the state diagram (Fig. 7). For voltage-dependent transitions the rate

constant was calculated according to: $k(V) = k(0\ mV) \exp(zFV/RT)$ where F, R and T have their usual thermodynamic meaning, $k(0\ mV)$ is the rate constant at 0 mV, and z is the equivalent charge moved between that state and the transition state. For the calculation of currents, the open channel *i-V* relationship was assumed to be ohmic.

Several of the figures include simulated current traces generated from the model to facilitate a comparison with the experimental traces. A consideration of the simulated data in those figures is deferred to the end of the Results section where the details of the gating model and its output are presented.

Results

Time course of the onset and wash-out of 4AP-induced inhibition of Kv4.2

With Kv4.2 channels expressed in *Xenopus* oocytes (Tseng et al., 1996) the reversibility of 4AP was quite limited and this prompted an investigation of the dynamics of the onset and offset of the 4AP in Kv4.2 channels expressed in HEK293 cells. The diary plot of Figure 1 shows the peak amplitudes of currents evoked during wash-in and wash-out of 1 mM, then 10 mM followed by a repeat application of 1 mM 4AP; bracketed numbers below data points in the graph refer to current traces shown above the graph. The holding potential (V_h) in the experiment was -80 mV. At the start of the experiment, two control (0 mM 4AP) currents evoked at 50 mV and separated by an interval of 20 s, had peak amplitudes of ~18.8 nA. Using the rapid perfusion system, the cell was then perfused with 1 mM 4AP for 60 s while the membrane voltage was maintained at V_h. Roughly 325 ms prior to switching back to control medium a 300 ms voltage step to 50 mV evoked at peak current of 10.4 nA, indicating a 45% decrease relative to the control currents. This decrease confirms that the onset the 4AP block is not contingent on membrane depolarization (Campbell et al., 1993; Castle and Slawsky, 1993; Tseng et al., 1996). Pulses to 50 mV applied at 0.05 Hz after switching back to control medium indicated that the peak amplitude of the current had recovered to 19.0 nA at t = 160 s, i.e., 80 s after the changeover. At that point a perfusion with 10 mM 4AP began and 40 s seconds after the changeover (t = 200 s) the peak current had decreased by ~70 % to 5.6 nA. Because 4AP block of transient outward currents is use-dependent (see below), voltage steps were suspended for roughly 80 s and then restarted 325 ms before returning to control solution. The amplitudes of the trace 3 and trace 4 currents were virtually the same, indicating that steady-state inhibition

with 10 mM 4AP could occur with a 20 s cycle length. Reversal of block by 10 mM 4AP was slower than with a 1 mM concentration but was nonetheless complete 100 s after wash-out (t = 380 s). Finally, switching back to 1 mM 4AP indicates that the onset of its block is comparable to that with 10 mM.

Inspection of the current traces in Figure 1 confirms two well-established effects of 4AP on transient outward currents (Thompson, 1982; Kehl, 1990; Castle and Slawsky, 1993; Tseng et al., 1996; Yeola and Snyders, 1997). First, the rise time of the current in the presence of the blocker is slowed, which is better seen in the traces evoked in 10 mM 4AP. Second, the decay of the current in 4AP is slowed. These two effects cause a crossover of the control and treated currents.

Steady-state concentration-response relationship

The concentration dependence of the steady-state block of Kv4.2 was determined with the awareness that the 4AP block of transient outward currents decreases, within limits, as the stimulus frequency increases. Consequently, the approach was to record control responses and then to switch to a known concentration of 4AP in the absence of any depolarizing pulses (V_h = -80 mV) for a period of 60 s with 4AP concentrations less than 2 mM and for 40 s with 2 mM and higher concentrations. Following this equilibration period, four test voltage-steps (P1-P4) to 50 mV each lasting for 300 ms were applied at a frequency of 0.8 Hz (cycle length of 1.25 s). A representative example of one such experiment is provided in Figure 5A which shows, superimposed, a control current as well as the test currents in 20 mM 4AP evoked by pulses 1-4. Note the slow risetime of the P1 current and that during the decay phase it crosses over the control current.

This section is restricted to a consideration of the effect of the 4AP concentration on the amplitude of the first of the four test pulses, which is taken as a measure of the steady-state or tonic block. A consideration of the basis for the increase of the current amplitude of P2 and subsequent pulses that is evident in Figure 5A is deferred until some details of the kinetics of 4AP unbinding (Fig. 3) and binding (Fig. 4) have been considered.

For the graph of Figure 2 the P1 test current amplitudes in 4AP concentrations ranging from 0.2 mM to 20 mM were normalized with respect to the average of the control and recovery

responses. A fit of the concentration dependence of the experimental, normalized P1 test currents to the Hill equation (*Eqn.* 1; solid line of Fig. 2) gave an estimate for the K_d, the concentration producing 50% of the maximal block, of 0.9 ± 0.07 mM. The best fit for the lower asymptote, which represents the normalized current in the presence of a saturating concentration of 4AP was 0.28 ± 0.02. In other words, the maximum block is roughly 72%. This value for the maximum block is related to the fact that current was measured at the peak and that relatively rapid unbinding of 4AP occurs during a step to 50 mV. The dashed line of Fig. 2 represents the best fit of the concentration-response data (∇) generated from the gating model (Fig. 7) and will be considered in the last section of the Results.

Increasing the concentration of 4AP also affected the time-to-peak of the current which in control cells was 2.87 ± 0.08 ms (n = 16). Although in 2 mM 4AP the effect was relatively small (3.14 ± 0.23, n = 4) there was a progressive increase of the time-to-peak to 10.4 ± 1.4 ms (n = 7) in 5 mM, to 15.9 ± 1.2 ms (n = 11) in 10 mM, and to 18.6 ± 1.1 ms (n = 3) in 20 mM.

The decay rate of the P1 test current was also concentration-dependent. In control cells, inactivation during a 300 ms step from -80 mV to 50 mV was well-fitted by a biexponential function where the faster component had a time constant (τ_f) of 7.8 ± 0.2 ms and accounted for 0.75 ± 0.008 (n = 19) of the total current decay and the slower component had a time constant (τ_s) of 40.2 ± 1.4 ms and a relative amplitude of 0.25 ± 0.008 (n = 19). With 4AP concentrations of 2 mM or less the current decay was biexponential with the main effect appearing to be a decreased contribution of the faster component and a slower relaxation of the second component. For example, with 2 mM 4AP τ_f was 10.2 ± 1.1 ms, τ_s was 51.9 ± 4.5 ms and the relative amplitudes of the two components were similar (0.473 and 0.527, respectively; n = 5). However, with higher concentrations the decay rate was well-fitted by a single exponential with a time constant of 51.9 ± 2.3 ms (n = 7) with 5 mM, 58.1 ± 1.9 ms (n = 10) with 10 mM, and 64.2 ± 3.6 (n = 3) with 20 mM. The basis for these changes of current decay is addressed in the section below dealing with the proposed model for 4AP block of Kv4.2 currents.

4AP unbinding from Kv4.2 channels at 50 mV

Castle and Slawsky (1993) proposed that in I_{to} channels of rat ventricular myocytes 4AP binds most strongly to closed states. In their study of macroscopic Kv4.2 currents Tseng et al. (1996) concluded that 4AP binds exclusively to closed states. A corollary of this state dependence of

binding is that depolarization triggers 4AP unbinding. To characterize the time dependence of the dissociation of 4AP during strong membrane depolarization a two-pulse protocol was used (Figure 3A). Briefly, for the first sweep an 8 ms conditioning pulse to 50 mV was used and its duration was doubled on successive sweeps up to 512 ms. To allow near complete recovery from inactivation ($\tau \approx 330$ ms) but limit the time available for 4AP rebinding to closed states, the interval at -80 mV between the end of the first pulse and the start of the second or test pulse was 1 s. The duration of the test pulse to 50 mV was 200 ms. For the exemplar traces of Figure 3A, which were recorded with internal 2.5 mM 4AP, the envelope of the peak test pulse currents (○) was well-fitted by a single exponential (solid line) with a time constant, $\tau_{unblock}$, of 50 ms. In seven cells in which it was measured $\tau_{unblock}$ at 50 mV was 41 ± 4.9 ms.

Given that the unblocking rate is equal to the sum of the on-rate ([4AP] * k_{on}) and the off-rate (k_{off}), then if 4AP is unable to bind to open channels at 50 mV then the unblocking rate is expected to be concentration-independent**.** Figure 3C shows the unblocking rate, calculated as the reciprocal of $\tau_{unblock}$, as a function of the 4AP concentrations ranging from 0.625 mM to 10 mM. A fit of the data points to a line gave a slope of -0.0002 ± 0.0004 mM^{-1} ms^{-1}, which was not significantly different from zero. This finding that the slope of the fitted line is concentration-independent suggests that little or no binding of 4AP occurs at 50 mV and that the unblocking rate is determined by k_{off}. This implies that with a 256 ms depolarization to 50 mV more than 99% of channels liganded prior to the conditioning pulse will become unliganded.

4AP binding at -80 mV

Determination of the time- and concentration-dependence of 4AP binding at -80 mV involved a two-pulse protocol in which the duration and the voltage of both pulses were the same (300 ms and 50 mV) and the interpulse interval of 50 ms for the first sweep was increased 1.5-fold on successive sweeps. The rationale for the protocol is that a 300 ms pre-pulse to 50 mV causes unbinding of 4AP and ultimately drives most of the channels to the closed-inactivated state (Bahring et al., 2001). Returning to -80 mV between pulses enables inactivated channels to recover to closed states and thence become targets for 4AP binding. Figure 4A shows representative traces recorded with internal 2.5 mM 4AP. The envelope of the peak test pulse

currents shows a biphasic pattern that was well-fitted by a rising (τ_1) and a decaying (τ_2) exponential function (*Eqn.* 4). For the traces of Figure 4A, the value for τ_1 was 259 ± 15 ms, which is a rough approximation of the time constant for recovery from inactivation, and τ_2, representing the time constant of 4AP binding at -80 mV, was 3.3 ± 0.3 s. Figure 4B shows the output of Scheme 4AP using the same voltage protocol and the same 4AP concentration as for the experimental data in Figure 4A.

For the graph of Figure 4C the blocking rate, calculated as the reciprocal of the time constant for 4AP binding (τ_2 of *Eqn.* 4), is plotted against the concentration of 4AP. Because the blocking rate is equal to the sum of the on-rate and the off-rate at -80 mV, and since only the on-rate has concentration dependence, the *y*-intercept value of 0.08 ± 0.03 s^{-1} estimates the value for k_{off}. Consistent with other reports (Castle and Slawsky, 1993; Tseng et al., 1996), the k_{off} of 0.00008 ms^{-1} (= 0.08 s^{-1}) at -80 mV is much smaller than it is at 50 mV (0.021 ± 0.001 ms^{-1}, Fig. 3C). The slope of the fitted line in Figure 4C gives a value of 0.08 ± 0.005 mM^{-1} s^{-1} for k_{on}.

Use-dependent unblock

Having established that the unbinding of 4AP from Kv4.2 channels is rapid and probably complete during a 300 ms step to 50 mV (Fig. 3), that k_{on} at -80mV is small and that binding proceeds only after recovery from inactivation (Fig. 4) a more tractable explanation for the increased amplitude of test currents evoked by P2-P4 in the traces of Fig. 5A is possible. The latter phenomenon is representative of reverse use-dependent block or, equivalently, use-dependent unblock, which denote that, within limits, an increase of stimulus frequency causes an increase of the peak current. This use-dependent increase of current arises for the following reasons. For the P1 current of Figure 5A, which was recorded after a 40 s sojourn at -80 mV in the presence of 20 mM 4AP, most of the channels are blocked at the start of the pulse to 50 mV (as suggested by the absence of a fast activating component of current) but the strong depolarization induces channels first to unblock and then to inactivate. When the membrane potential is returned to -80 mV channels recover from inactivation and binding of 4AP to closed channels proceeds, albeit slowly, and, because a depolarizing pulse is applied before the binding

reaction achieves the steady state, more channels are in closed-unbound states and the test current is larger.

Since the binding rate is proportional to the 4AP concentration (i.e., [4AP] x k_{on}(-80 mV)) the extent of 4AP binding at the end of the 950 ms interval between pulses is governed by the 4AP concentration. This is confirmed in the graph of Figure 5C which plots the concentration dependence of the mean normalized experimental P2-P4 amplitudes (○) evoked using the voltage protocol described for Figure 5A. These data indicate that increasing the stimulus frequency to 0.8 Hz causes an apparent increase of the K_d for the block such that 1 mM 4AP caused only ~8% inhibition as opposed to ~40% inhibition for tonic block (Fig. 2) and with 20 mM 4AP this changed from ~70% inhibition for tonic block to ~42% inhibition at 0.8 Hz. As will be discussed, the experimental data obtained using the voltage protocol of Figure 5A are reasonably replicated by Scheme 4AP (Fig. 5B and ∇ in Fig. 5C).

Voltage dependence of the relative block of Kv4.2

The aim of this section is to describe the effect of varying the membrane potential in the range of -80 to -30 mV on test current amplitude in the presence of different concentrations of 4AP. The rationale for the voltage protocol (see Fig. 6B), which is predicated on the mutual exclusivity of inactivation and 4AP block (Fig. 4 and see Introduction), was to apply a 30 s depolarizing conditioning step (P1) to increase the extent of channel inactivation and in doing so decrease the proportion of closed-bound channels. At the end of the conditioning pulse the voltage was stepped to -80 mV for 1.3 s to allow the inactivated channels to recover to closed states prior to the 300 ms test pulse to 50 mV. Representative responses in the presence of 10 mM 4AP (Fig. 6B) show that the currents following conditioning pulses of -80 mV and -70 mV are superimposed, that a step to -60 mV slightly increases the risetime of the current but has no substantial effect on the peak current, and that the maximal test current is seen following conditioning pulses to either -40 mV or -30 mV. Test currents such as these were normalized according to *Eqn.* 5 to give the relative block, which was then plotted against the potential of the conditioning pulse (P1). Figure 6A shows the best fit of a Boltzmann function (*Eqn.* 6) to the relative block with 2 mM 4AP (V_{half} = -56.4 ± 0.4 mV, s = 4.2 ± 0.3 mV, n = 6) and 10 mM 4AP (V_{half} = -51.8 ± 0.2 mV, s = 3.3 ± 0.4 mV, n = 10). As noted by Thompson (1982) and others, the

relative block curves have a shape similar to that for the availability curve (dashed line of Fig. 6A) but show a concentration-dependent rightward shift of the V_{half}, the voltage at which the relative block is half-maximal (see Table 1 for the experimental and simulated values for V_{half} and *s*). Figure 6C, D show the outcome of the relative block voltage protocol in the gating model and are discussed along with other simulated data in the following section.

A model of 4AP block of Kv4.2

The effect of 4AP on Kv4.2 currents has not been modelled previously, however several gating models have been proposed to account for the block by 4AP of transient outward currents such as I_{to} and I_A. The first, a 5-state model incorporating both closed and open channel block (Thompson, 1982), and a related 4-state model engendering only closed state block (Kehl, 1990), reproduced several of the properties of 4AP block but were predicated on the assumption, now known to be incorrect, that a single inactivation process was strictly coupled to channel opening. A subsequent 10-state model (Campbell et al., 1993) reproduced many of the features of block of I_{to} in ventricular myocytes and incorporated closed state binding of 4AP as well as closed state inactivation but here too some of the assumptions underpinning the gating scheme are now known to be incorrect. For example, the model assumed that closed state inactivation was in series with open channel inactivation and, by extension, that the two were conformationally related, but it has been shown that CSI persists after fast open-state inactivation has been removed (Jerng and Covarrubias, 1997).

Figure 7 shows the gating scheme, referred to subsequently as Scheme 4AP, used to simulate the effect of 4AP on Kv4.2 currents. The middle and lower rows of the gating scheme are the same as for Model 2 of Bahring et al. (2001) that was shown to replicate biophysical properties of Kv4.2 ionic currents such as closed state inactivation, recovery from CSI that bypasses the open state, and three components of inactivation during a 2.5 s depolarization to 40 mV. In this study a third component of inactivation was not detectable with a 300 ms step to 50 mV but there was good concordance between the mean values for and the relative amplitudes of τ_f (7.8 ms and 0.75) and τ_s (40.2 ms and 0.25) and those reported by Bahring et al. (2001) for τ_1 (11.0 ms and 0.73) and τ_2 (50 ms and 0.23). An allosteric factor *f*, which is required to satisfy microscopic

reversibility, and the rate constants were unchanged with one exception: the value for k_{ic} was decreased from 0.1 s^{-1} to 0.02 s^{-1} to give a time constant for recovery from inactivation at -80 mV of 330 ± 8 ms, which is a good approximation of the experimentally-measured value of 330 ± 14 ms (not shown). With k_{ic} = 0.02 s^{-1} the mid-point of the availability or steady-state inactivation curve was -61.7 ± 0.1 mV, which is left-shifted by roughly 4 mV with respect to the mean experimental value. Simulated and experimental availability curves had slope factors, determined by the fit to the Boltzmann function (*Eqn.* 6), of 5.3 ± 0.2 ms and 5.4 ± 0.2 ms, respectively (Table 1).

The middle row of Scheme 4AP includes an activation pathway that presumes a tetrameric channel construct comprising four identical but independent subunits, a concerted opening transition from the fully-activated-not-open or pre-open closed state (C_4), and open channel inactivation arising from N-type inactivation in series with C-type inactivation. Downward and upward transitions between the middle and lower row of states represent CSI and recovery from CSI, respectively. Transitions between states in the lower row represent activation and deactivation of closed-inactivated channels.

Block by 4AP was incorporated by the addition of six 4AP-bound states (C_0B to OB, top row of Fig. 7). Binding of 4AP is restricted to closed states (C_0B to C_4B) and the on-rate is the product of the association rate constant (k_{on}), in mM^{-1} s^{-1}, and the 4AP concentration, in mM. This assumption of a 1:1 binding stoichiometry is consistent both with the concentration-response relationship reported here (Fig. 2) and by others for Kv4-based rapidly inactivating currents (Castle and Slawsky, 1993; Tseng et al., 1996) as well as for the block of other classes of Kv channels (e.g., Kirsch and Drewe, 1993). Based on the data of Figure 3C the open state is presumed to have no affinity for 4AP. In the *Shaker* channel the movement of the cationic form of 4AP onto its binding site is affected by the membrane electric field (*e*-fold change per 58 mV at 20° C) however the binding reaction is assumed here not to be directly voltage-dependent. To satisfy microscopic reversibility it was also necessary to include an allosteric factor, *g*, both in the vertical transition rates representing 4AP binding and unbinding between the middle and top rows of Scheme 4AP, and in the horizontal transitions representing voltage sensor activation between closed-bound states. Several assumptions were made to decrease the number of free

variables in the model. The first is that voltage sensor movement is unchanged in 4AP-bound closed channels. There are no data available on the effect of 4AP on Kv4.2 gating currents, but this assumption is consistent with numerical modelling showing that the features of the 4AP block of the delayed rectifier of the SGA can be replicated without the need to change activation gating kinetics (Yeh et al., 1976a), and that SGA delayed rectifier gating currents (Spires and Begenisich, 1989) as well as *Shaker* gating currents (McCormack et al., 1994; Armstrong and Loboda, 2001) are unaffected by 4AP. To satisfy this presumption that the activation kinetics of closed-bound channels are the same as for closed-unbound channels it was necessary to constrain the allosteric factor *g* to be one. Because *g* also appears in the calculation of the on- and off-rates for 4AP binding, another consequence of setting *g* to one is that the affinity of 4AP for each of the five closed states (C_0 to C_4) is the same. Some support for this assumption has been provided by Campbell et al. (1993) who found that the affinities were not substantially different for at least two of the closed states. Constraining *g* to be one means that it could be eliminated from the gating scheme, but it is nonetheless included to give an appreciation of the fact that a value for *g* greater than or less than one affects both the activation kinetics of closed-bound states as well as the relative affinities of the closed states for 4AP.

In all the previous models of the 4AP block of transient outward currents (Thompson, 1982; Kehl, 1990; Campbell et al., 1993), 4AP dissociation was assumed to precede channel opening. When this same condition was imposed in Scheme 4AP by eliminating the OB state there was a concentration-dependent decrease of the peak current evoked by a step from -80 mV to 50 mV however the characteristic apparent slowing of activation and inactivation that culminate in the crossover of control and treated currents did not occur, regardless of the value for *g* (not shown). Consequently, to replicate the effects of 4AP on Kv4.2 current kinetics it was necessary to include transitions from the closed-blocked to the open-blocked to the open state (corresponding to C_4B to OB to O in Fig. 7). In the case of delayed rectifier-like K^+ channels two different approaches have been used to model the time course of these transitions. For the 4AP block of the SGA delayed rectifier, unbinding of 4AP from the open state was assumed to be the rate-limiting step (Yeh et al., 1976a) whereas for the block of inactivation-removed *Shaker* channels the opening step was assumed to be rate-limiting (Armstrong and Loboda, 2001). With Scheme 4AP either of these approaches, normal opening and slow unblock or slow opening and rapid unblock, produced identical outcomes (not shown) and, for reasons that are discussed later, the

choice was made to set the unblocking of open-bound (OB) channels as the rate-limiting step (Table 2).

Since, with the one exception noted in Methods, the transition rates for the middle and bottom row of states of Scheme 4AP were constrained to be the same as those reported by Bahring et al. (2001), and in light of the constraint that the allosteric factor *g* be fixed at one, the addition of six 4AP-bound states used to generate Scheme 4AP added five variables (k_{on}, k_{off}, k_{cb_ob}, k_{ob_cb} and k_{ob_o}), of which two, k_{on} and k_{off} at -80 mV, were constrained by experimental data. Table 2 lists the values of the simulation variables.

Overall, Scheme 4AP reproduces the time- and concentration-dependence of the effect of 4AP on Kv4.2 currents reasonably well. The simulated values for the concentration-response relationship (dashed line of Fig. 2) yield a K_d of 0.88 ± 0.06 mM, a Hill coefficient (*h*) of 1.16 ± 0.07 and a base of 0.25 ± 0.02, which represents the proportion of the normalized peak current persisting in a saturating concentration of 4AP. These correspond well with the experimental values in Figure 2 (0.9 ± 0.07 mM, 1.2 ± 0.07 and 0.28 ± 0.02, respectively) and are in accord with those reported for Kv4.2 channels expressed in *Xenopus* oocytes (K_d = 1.5 mM, base ≈0.28) (Tseng et al., 1996).

The concentration-dependence of the decay kinetics is also replicated by the model. For example, in the absence of 4AP the decay during a 300 ms step to 50 mV was well-fitted by a biexponential function with time constants of 10.3 and 47.3 ms (versus experimental values of 7.8 ± 0.2 ms and 40.2 ± 1.4 ms), and in 10 mM 4AP the decay of the modelled current was well-fitted by a monoexponential function with a time constant of 65.6 ms (versus the experimental value of 58.1 ± 1.9 ms (*n* = 10)). This change of the decay rate with high concentrations of 4AP appears to arise primarily from the much slower delivery of channels to the N-type type inactivation process (OI_1 in Scheme 7). A similar explanation has been proposed to account for a comparable action of 4AP to slow C-type inactivation in *Sh*IR channels (Castle et al., 1994b).

Using a voltage protocol identical to that of Figure 3A, the model accurately replicates the time dependence of the channel unblock at 50 mV (Fig. 3B, τ_{exp} = 50 ± 2.4 ms versus τ_{sim} = 51.6 ± 1.2

ms) as well as a ~2.1-fold increase the test pulse current, relative to the peak of the pre-pulse current, following the 256 ms and 512 ms pre-pulses. Likewise, in Figure 4A, B there is good agreement between the time-dependence of recovery from inactivation (which is underestimated by the fitting process) (τ_{exp} = 259 ± 15 ms versus τ_{sim} = 259 ± 8 ms) and the onset of block (τ_{exp} = 3.29 ± 0.27 s versus τ_{sim} = 3.9 ± 0.37 s). The maximum test current, expressed as a proportion of the prepulse current, was 2.1 and 2.4 for the experimental and simulated data, respectively.

The model also replicates reverse use-dependent block in which the proportion of channels blocked by 4AP is decreased by increasing the frequency of test depolarizations. Figure 5B shows there is a reasonable correlation, both in terms of peak amplitude and the kinetics of the currents, between simulated traces presented in the same format, using the same voltage protocol and with the same 4AP concentration as for the experimental traces in Figure 5A. And, in Figure 5C a plot of the experimentally measured (○) and the simulated (∇) relationship between the average peak amplitude of the P2-P4 test currents and the concentration of the 4AP, shows that the two are similar.

Finally, the graph of Figure 6C shows the effect of 2 mM and 10 mM 4AP on the relationship between the relative block and the voltage of a 30 s conditioning pre-pulse (P1). Data points of Figure 6C were measured from simulated currents such as those in Figure 6D. In Figure 6C the dashed line represents the simulated control steady-state availability curve (V_{half} = -61.6 ± 0.1 mV, s = 5.3 ± 0.2 mV) for the model and the solid lines represent the best fit of the data to a Boltzmann relationship (*Eqn.* 6) in 2 mM 4AP (V_{half} = -56.6 ± 0.2 mV, s = 4.1 ± 0.2 mV) and 10 mM 4AP (V_{half} = -50.8 ± 0.1 mV, s = 2.7 ± 0.1 mV). This indicates that with respect to the simulated availability curve, the V_{half} of the simulated relative block relationship is right-shifted by ~5.1 mV in 2 mM 4AP and by ~10.9 mV in 10 mM 4AP; the simulated curve in 10 mM 4AP is right shifted by 5.8 mV with respect to the curve in 2 mM 4AP. Table 1 summarizes the experimental and simulated values for V_{half} and s and indicates there is reasonable agreement between the two data sets.

Discussion

Comparison to a previous study of the block of Kv4.2 by 4AP

JPET Fast Forward. Published on September 1, 2017 as DOI: 10.1124/jpet.117.243097
This article has not been copyedited and formatted. The final version may differ from this version.

The experimental data are in good agreement with those reported for Kv4.2 channels expressed in *Xenopus* oocytes (Tseng et al., 1996). The concentration-response relationship gave values for the K_d of 0.9 mM (Fig. 2) versus 1.5 mM and both indicated a value of ~70% for the maximal block of the current with a saturating concentration of 4AP. And the values for $\tau_{unblock}$ in the two studies are virtually the same: 41 ± 4.9 ms with a conditioning pulse to 50 mV versus 42 ± 6 ms with a conditioning pulse to 60 mV. It was suggested that $\tau_{unblock}$ at positive voltages was independent of the 4AP concentration and data supporting that notion were obtained in this study (Fig. 3C). With respect to the relative block (Fig. 6), the experimental values (Table 1) for the right shift of the V_{half} going from 2 mM to 10 mM were comparable, i.e., 4.4 mV versus 5.1 mV, as were the values for *s* with 4AP concentrations of 2 mM (4.1 mV versus 4.1 mV) and 10 mM (3.3 mV versus 3.7 mV). Although the estimates of the unblocking rates at -80 mV (0.08 ± 0.03 s^{-1} (Fig. 4C) versus 0.062 s^{-1}) are similar, there is a substantial difference in the association rate constant of 0.08 ± 0.005 mM^{-1} s^{-1} (Fig. 4C), which is 6.6-fold larger than that reported by Tseng et al. (1996). Overall, the similarity of the data reported in this study and by Tseng et al. (1996) suggests that the values used to constrain Scheme 4AP are reasonable.

Comparison to the block of I_{to} by 4AP

In cardiac myocytes I_{to} is mediated by Kv4 channels co-expressed with accessory subunits such as Kv channel interacting proteins and dipeptidyl aminopeptidase-like proteins (Birnbaum et al., 2004; Niwa and Nerbonne, 2010). Because a major effect of the accessory subunits is to slow the fast phase of inactivation during a strong depolarizing pulse and to accelerate recovery from inactivation, it is of some interest to compare the effects of 4AP on Kv4.2 versus cardiac I_{to}. Qualitatively, the features of the block of I_{to} by 4AP are the same as those noted above but there are some quantitative differences. These include a higher affinity for 4AP − K_d ~0.2 mM (Castle and Slawsky, 1993) versus 1 mM, and an association rate constant (k_{on}) of 0.2 mM^{-1} s^{-1} at -70 mV which is 2.5 and 17-fold larger, respectively, than that measured at -80 mV in this study and by Tseng et al. (1996). Despite the wide variation in these k_{on} values, the dissociation rate constants (k_{off}) from the same three labs are quite comparable (0.09 s^{-1} at -70 mV, 0.08 s^{-1} and 0.062 s^{-1} at -80 mV). In light of the similarity of the k_{off} values at -70 to -80 mV, it is surprising that at 50 mV the value for k_{off} in ferret myocytes (Campbell et al., 1993) is roughly 5-fold smaller for I_{to} than the value of 25 s^{-1} measured in Kv4.2 channels (Fig. 3C). Despite the fact that

JPET Fast Forward. Published on September 1, 2017 as DOI: 10.1124/jpet.117.243097
This article has not been copyedited and formatted. The final version may differ from this version.

k_{off} at depolarized potentials is markedly smaller in I_{to} it shares with Kv4.2 (Fig. 3C) the property of being concentration-independent (Castle and Slawsky, 1993) and provides some additional support for the assumption in the proposed gating model that open Kv4.2 channels do not bind 4AP.

Comparison to the 4AP block of other Kv channels

Many of the features of the block of Kv4.2 by 4AP are similar to those reported for the delayed rectifier current, both in the SGA (Yeh et al., 1976a; Kirsch et al., 1986) and its cell bodies in the giant fibre lobe (GFL) (Jerng and Gilly, 2002), which is putatively mediated by channels of the Kv1 class (Rosenthal et al., 1996). These features include closed channel block at a membrane voltage as low as -100 mV (Jerng and Gilly, 2002), implying that binding can occur in the fully deactivated closed state, and a relief of the block ($\tau_{unblock}$ = 10-20 ms) during membrane depolarization, i.e., use-dependent unblock. Indeed, aside from the fact that Scheme 4AP included inactivation gating, it is qualitatively quite similar to that used by Yeh et al. (1976a). This similarity of these two gating models includes the assumption that activation gating is unaffected by 4AP, as has been shown directly by gating current measurements in the SGA (Spires and Begenisich, 1989) and *Shaker* (McCormack et al., 1994; Loboda and Armstrong, 2001).

The k_{on} for 4AP in open Kv3.1 channels is 2.1 x 10^4 M^{-1} s^{-1} (Kirsch and Drewe, 1993) and that for the open *Shaker* channel at 0 mV is 1.4 x 10^7 M^{-1} s^{-1} (Armstrong and Loboda, 2001). In the case of the open *Shaker* channel it is worth noting that, because of a very large k_{off}, the K_d(0 mV) is quite large, 57 mM, and thus open Kv4.2 and *Shaker* channels share the property of a low affinity for 4AP. These values for the k_{on} for open channels contrast sharply with those reported for closed state block. In Kv4.2 at -80 mV the k_{on} of 80 M^{-1} s^{-1} (Fig. 4C) compares well to the value of 100 M^{-1} s^{-1} for the binding to closed Kv3.1 channels (Kirsch and Drewe, 1993). Interestingly, in Kv3.1 channels, which demonstrate both closed and open channel block, the k_{on} for closed channels is roughly 200-fold smaller than for open channels. Given that the concentration-block relationship for the block of Kv3.1, as in other Kv channels (McCormack et al., 1994) and in this study (Fig. 2), is consistent with a 1:1 binding model, Kirsch and Drewe (1993) proposed there was a single binding site (as opposed, for example, to a site on each of the four α-subunits) on the cytoplasmic side of the conduction pathway and that the difference in the

JPET Fast Forward. Published on September 1, 2017 as DOI: 10.1124/jpet.117.243097
This article has not been copyedited and formatted. The final version may differ from this version.

rates of closed and open channel block simply reflected differing accessibilities to that site. A possible explanation for the divergence of k_{on} for open and closed channel block is guarding of the binding site by the activation gate, which is formed by the convergence of S6 segments on the cytoplasmic side of the pore. In *Shaker*, Kv3.1 and Kv2.1 channels with an open activation gate 4AP has an on-rate that approaches that for pore blockers such as TEA^+ and it is conceivable that the very small k_{on} measured at rest in Kv3.1 and in Kv4.2 is due a very small open probability at rest.

The 4AP block of Kv4.2 could be modelled either by assuming slow unbinding of 4AP from open-bound channels, as proposed for the block of the SGA delayed rectifier and Kv3.1 channels (Yeh et al., 1976a; Kirsch and Drewe, 1993), or that 4AP stabilized the pre-open closed state such that the rate-limiting step of channel opening preceded rapid channel unblock (Armstrong and Loboda, 2001),. The latter mechanism was simulated in Scheme 4AP (not shown) by decreasing the rate of the C_4B to OB transition from 400 s^{-1} to 18 s^{-1} and destabilizing the open state by increasing the rate of the OB to C_4B transition from 1100 s^{-1} to 3544 s^{-1}; once open, the off-rate of 4AP was assumed to be 10^5 s^{-1}. However, because the P_o of closed-bound states would decrease relative to closed-unbound channels, an expected consequence of this gating scheme is that recovery from resting block would acquire some degree of use-dependence. This remains to be definitively studied using fast application of 4AP to inside-out patch recordings. At this time a mechanism of action similar to that proposed for *Shaker* channels (Armstrong and Loboda, 2001) cannot be ruled out and indeed has some appeal given that CSI has been proposed to involve a dissociation or slippage between voltage sensor movement and activation gate opening (Dougherty et al., 2008; Bahring and Covarrubias, 2011). On the other hand, the finding that k_{on} in Kv4.2 is "independent of the membrane voltage in the range of -80 to -120 mV" (Tseng et al., 1996) is a plausible argument against a dependence of tonic block on a small P_o at rest. Jerng and Gilly (2002) have also expressed reservations about ascribing the potent resting block of the GFL delayed rectifier current versus the virtual absence of resting block in sqKv1A to a difference in the resting P_o.

In summary, the binding of 4AP to closed channels causes a concentration dependent block of Kv4.2 currents that can be manifest during a depolarizing step as an apparent slowing of activation and a delayed onset of inactivation that can cause the test current to cross over the

control current. 4AP appears to have a very low or no affinity for open channels, and 4AP binding and inactivation are mutually exclusive processes. These features are replicated in a gating scheme in which 4AP is assumed to have no effect on gating current and in which there is either slow unbinding from open channels or a biasing of the concerted opening/closing step more strongly to the pre-open closed state. Whether the small k_{on} for closed state block of Kv4.2 channels is due to a low open probability at rest remains an unanswered question.

Acknowledgements

I am grateful to Zhuren Wang for expert technical assistance.

Authorship Contributions

Participated in research design: Kehl

Conducted experiments: Kehl

Contributed analytic tools: Kehl

Performed data analysis: Kehl

Wrote the manuscript: Kehl

References

Armstrong CM (1971) Interaction of tetraethylammonium ion derivatives with the potassium channels of giant axons. *J Gen Physiol* **58**:413-437.

Armstrong CM (1997) A closer picture of the K channel gate from ion trapping experiments. *J Gen Physiol* **109**:523-524.

Armstrong CM and Loboda A (2001) A model for 4-aminopyridine action on K channels: similarities to tetraethylammonium ion action. *Biophys J* **81**:895-904.

Bahring R, Boland LM, Varghese A, Gebauer M and Pongs O (2001) Kinetic analysis of open- and closed-state inactivation transitions in human Kv4.2 A-type potassium channels. *J Physiol* **535**:65-81.

Bahring R and Covarrubias M (2011) Mechanisms of closed-state inactivation in voltage-gated ion channels. *J Physiol* **589**:461-479.

Birnbaum SG, Varga AW, Yuan LL, Anderson AE, Sweatt JD and Schrader LA (2004) Structure and function of Kv4-family transient potassium channels. *Physiol Rev* **84**:803-833.

Campbell DL, Qu Y, Rasmusson RL and Strauss HC (1993) The calcium-independent transient outward potassium current in isolated ferret right ventricular myocytes. II. Closed state reverse use-dependent block by 4-aminopyridine. *J Gen Physiol* **101**:603-626.

Castle NA, Fadous S, Logothetis DE and Wang GK (1994a) Aminopyridine block of Kv1.1 potassium channels expressed in mammalian cells and *Xenopus* oocytes. *Mol Pharmacol* **45**:1242-1252.

Castle NA, Fadous SR, Logothetis DE and Wang GK (1994b) 4-aminopyridine binding and slow inactivation are mutually exclusive in rat Kv1.1 and *Shaker* potassium channels. *Molecular Pharmacology* **46**:1175-1181.

Castle NA and Slawsky MT (1993) Characterization of 4-aminopyridine block of the transient outward K^+ current in adult rat ventricular myocytes. *J Pharmacol Exp Ther* **264**:1450-1459.

Cheng YM, Fedida D and Kehl SJ (2010) Kinetic analysis of the effects of H^+ or Ni^{2+} on Kv1.5 current shows that both ions enhance slow inactivation and induce resting inactivation. *J Physiol* **588**:3011-3030.

Colquhoun D and Hawkes AG (2011) A Q-matrix cookbook, in *Single Channel Recording* pp 589-633, Plenum Press, N.Y.

Dougherty K, De Santiago-Castillo JA and Covarrubias M (2008) Gating charge immobilization in Kv4.2 channels: the basis of closed-state inactivation. *J Gen Physiol* **131**:257-273.

Doyle DA, Morais CJ, Pfuetzner RA, Kuo A, Gulbis, Jm, Cohen SL, Chait BT and MacKinnon R (1998) The structure of the potassium channel: molecular basis of K^+ conduction and selectivity. *Science* **280**:69-77.

Fiset C, Clark RB, Shimoni Y and Giles WR (1997) *Shal*-type channels contribute to the Ca^{2+}-independent transient outward K^+ current in rat ventricle. *J Physiol* **500**:51-64.

Jerng HH and Covarrubias M (1997) K^+ channel inactivation mediated by the concerted action of the cytoplasmic N- and C-terminal domains. *Biophys J* **72**:163-174.

Jerng HH and Gilly WF (2002) Inactivation and pharmacological properties of sqKv1A homotetramers in *Xenopus* oocytes cannot account for behavior of the squid "delayed rectifier" K^+ conductance. *Biophys J* **82**:3022-3036.

Kehl SJ (1990) 4-aminopyridine causes a voltage-dependent block of the transient outward current in rat melanotrophs. *J Physiol* **431**:512-528.

Kehl SJ, Fedida D and Wang Z (2013) External Ba^{2+} block of Kv4.2 channels is enhanced in the closed-inactivated state. *Am J Physiol Cell Physiol* **304**:C370-C381.

Kirsch GE and Drewe JA (1993) Gating-dependent mechanism of 4-aminopyridine block in two related potassium channels. *J Gen Physiol* **102**:797-816.

Kirsch GE and Narahashi T (1983) Site of action and active form of aminopyridines in squid axon membranes. *J Pharmacol Exp Ther* **226**:174-179.

Kirsch GE, Yeh JZ and Oxford GS (1986) Modulation of aminopyridine block of potassium currents in squid axon. *Biophys J* **50**:637-644.

Loboda A and Armstrong CM (2001) Resolving the gating charge movement associated with late transitions in K channel activation. *Biophys J* **81**:905-916.

McCormack K, Joiner WJ and Heinemann SH (1994) A characterization of the activating structural rearrangements in voltage-dependent *Shaker* K^+ channels. *Neuron* **12**:301-315.

Niwa N and Nerbonne JM (2010) Molecular determinants of cardiac transient outward potassium current (I(to)) expression and regulation. *J Mol Cell Cardiol* **48**:12-25.

Rosenthal JC, Vickery RG and Gilly WF (1996) Molecular identification of SqKv1A - A candidate for the delayed rectifier K channel in squid giant axon. *J Gen Physiol* **108**:207-219.

Spires S and Begenisich T (1989) Pharmacological and kinetic analysis of K channel gating currents. *J Gen Physiol* **93**:263-283.

Thompson S (1982) Aminopyridine block of transient potassium current. *J Gen Physiol* **80**:1-18.

Thompson SH (1977) Three pharmacologically distinct potassium channels in molluscan neurones. *J Physiol* **265**:465-488.

Tseng GN, Jiang M and Yao JA (1996) Reverse use dependence of Kv4.2 blockade by 4-aminopyridine. *J Pharmacol Exp Ther* **279**:865-876.

Yeh JZ, Oxford GS, Wu CH and Narahashi T (1976a) Dynamics of aminopyridine block of potassium channels in squid axon membrane. *J Gen Physiol* **68**:519-535.

Yeh JZ, Oxford GS, Wu CH and Narahashi T (1976b) Interactions of aminopyridines with potassium channels of squid axon membranes. *Biophys J* **16**:77-81.

Yeola SW and Snyders DJ (1997) Electrophysiological and pharmacological correspondence between Kv4.2 current and rat cardiac transient outward current. *Cardiovascular Research* **33**:540-547.

Footnotes

Supported by a Discovery Grant to S. Kehl from the Natural Sciences and Engineering Research Council of Canada.

Legends for Figures

Fig. 1. A diary plot of the peak Kv4.2 current tracking the time course of the onset and offset of externally applied 1 mM and 10 mM 4AP. Solutions changes and their timing are indicated by the horizontal lines in the graph. Bracketed numbers below select data points in the plot refer to the corresponding current traces above. See text for experimental details. The current traces in 1 mM and 10 mM 4AP crossover the control current and a prominent slowing of the activation is evident in10 mM 4AP. In these and subsequent current traces the dotted line indicates the zero current level.

Fig. 2. The experimental and simulated concentration-response relationship for the interaction of 4AP with Kv4.2 channels. Experimental data (•)(mean ± SEM) representing tonic block were generated from the peak current evoked by a 300 ms step to 50 mV following an interval of 60 s (< 2 mM) or 40 s (2 mM and higher) at the holding potential of -80 mV. The peak current, measured once the binding equilibrium was reached, was normalized to the average of the control and recovery currents. The solid line indicating the best fit of the data points to the Hill equation (*Eqn*. 1) was obtained with K_d = 0.9 ± 0.07 mM, h = 1.2 ± 0.07 and *base* = 0.28 ± 0.02.

JPET Fast Forward. Published on September 1, 2017 as DOI: 10.1124/jpet.117.243097
This article has not been copyedited and formatted. The final version may differ from this version.

Concentration-response data (∇) generated from Scheme 4AP (Fig. 7) over the same range of 4AP concentrations was well-fitted by the *Eqn.* 1 (dashed line) with K_d = 0.88 ± 0.06 mM, h = 1.16 ± 0.07 and *base* = 0.25 ± 0.02.

Fig. 3. The time-dependence of the dissociation of 4AP from Kv4.2 channels during a depolarization to 50 mV. (A) For the experimental traces a prepulse to 50 mV with a duration that varied from 8 to 512 ms was followed, after a fixed 1 s interval at -80 mV, by a step back to 50 mV for 200 ms. The 1 s interpulse interval at -80 mV is sufficient to allow near complete recovery from inactivation but is too short to allow substantial re-binding of 4AP, which was present at a concentration of 2.5 mM in the internal solution. The envelope of peak amplitudes of test currents is well-fitted by a single exponential with a time constant of 50 ms (SD = 2.4 ms). As indicated by the overlap of the pre-pulse currents, a 40 s interval between sweeps allowed steady-state block to be re-established. (B) For traces simulated using Scheme 4AP (Fig. 7) the voltage protocol and 4AP concentration were the same as for panel A. (C) A plot of the experimental unblocking rate (ms^{-1}) at 50 mV versus the concentration of 4AP, which varied from 0.625 to 10 mM. The slope of the line fitted to the data does not differ from zero and signifies that the unblocking rate is determined by the dissociation rate, implying that open Kv4.2 channels have little or no affinity for 4AP.

Fig. 4. The time- and concentration-dependence of the 4AP binding at -80 mV. (A) The first or conditioning pulse of a two-pulse protocol shown below the current traces triggered the unbinding of 4AP (cf. Fig. 3A) which then allowed inactivation to proceed. Using *Eqn.* 4, a fit of the envelope of the peak test currents (○) evoked by stepping to 50 mV indicated a time constant (τ_1) for recovery from inactivation of 259 ms and, with 2.5 mM 4AP in the internal solution, a time constant (τ_2) of 3.3 s for the rebinding of 4AP to closed channels at -80 mV. The dashed line denotes the mean of the peak currents evoked by the conditioning pulse. (B) Simulated currents using 2.5 mM 4AP and the same voltage protocol gave values of 259 ms and 3.9 s, respectively, for τ_1 and τ_2. See the last section of Results for details. (C) Data obtained using the same experimental protocol as in panel A with concentrations of 4AP ranging from 0.625 to 10 mM. The slope of the line fitted to the data indicates a value for k_{on} of 0.08 mM^{-1} s^{-1}, and the y-intercept indicates a value for k_{off} of 0.08 s^{-1}.

Fig. 5. Increasing the frequency of depolarizing pulses decreases 4AP block. (A) The voltage protocol shown above the current traces consisted of a 40 to 60 s period at -80 mV followed by four 300 ms pulses to 50 mV separated by a 950 ms interpulse interval at -80 mV. The peak amplitude of the first pulse (P1), taken to represent tonic block, was used to generate the concentration-response relationship of Figure 2. Current traces recorded in the continuous presence of external 20 mM 4AP show a 56% increase of the peak current of pulses 2-4 relative to pulse 1, as well as a marked increase of the activation rate. (B) The output of Scheme 4AP using the same voltage protocol and 20 mM 4AP reproduces the experimental data reasonably well. (C) The mean (± SE) of the peak currents evoked by P2-P4 expressed as a proportion of the control current versus the 4AP concentration. There is reasonable concordance of the

JPET Fast Forward. Published on September 1, 2017 as DOI: 10.1124/jpet.117.243097
This article has not been copyedited and formatted. The final version may differ from this version.

experimental (○) and simulated (∇) relationship except with the higher concentrations of 4AP where the simulated currents tend to show slightly less potentiation than the experimental currents. A comparison to the data for the tonic block (•), taken from Figure 2, indicates that increasing the stimulus frequency causes an apparent right-shift of the concentration-response curve. The Boltzmann function fitted to the data for the experimental 0.8 Hz block has a V_{half} of 10.7 ± 0.45 mM and a base of 0.41 ± 0.1 with the rate fixed at 1.2.

Fig. 6. Changing the holding potential between -80 and -30 mV causes a concentration-dependent decrease of the 4AP block. (A) The experimental relative block, calculated according to *Eqn.* 5, as a function of the P1 (conditioning) voltage of the stimulus protocol, which is shown uppermost in panel B. With respect to the control availability curve, the V_{half} derived from a fit of the data to a Boltzmann function (*Eqn*. 6) shifted by 3.1 mV and 7.5 mV in 2 mM and 10 mM 4AP, respectively. The shift of the V_{half} was associated with a decrease of the slope factor from the mean control value of 5.4 mV to 4.2 mV and 3.3 mV in 2 and 10 mM 4AP, respectively. (B) Representative experimental P2 currents evoked in 10 mM 4AP at the indicated P1 voltages. (C) The relative block simulated using Scheme 4AP and using the same voltage protocol and 4AP concentrations used to generate the data of panel A. Although the V_{half} for the simulated availability curve is slightly left-shifted with respect to the experimental availability curve (see Table 1), the right shift of V_{half} by 5 mV in 2 mM 4AP and by 10.8 mV in 10 mM 4AP compares reasonably well to that observed experimentally. With 2 mM 4AP the decrease of *s* by 1.2 mV was the same for the experimental and the simulated data, and with 10 mM 4AP the decrease of *s* in the simulation was 2.6 mV versus 2.1 mV for the experimental data (cf. Table 1). (D) Simulated current traces generated using the same voltage protocol and 4AP concentration as in panel B and from which the relative block curve in 10 mM 4AP in panel C was derived.

Fig. 7. A model, referred to as Scheme 4AP, of the block of Kv4.2 by 4AP. The model was built around the gating scheme referred to as Model 2 in Bahring et al. (2001), which comprises the middle and lower rows of channel states. Activation of closed channels (middle row) involves voltage sensor movement in each of the subunits of the tetrameric structure and leads to the activated-not-open or pre-open closed state (C_4). Channel opening and channel closing result from concerted (highly cooperative) transitions. In the same row, two forms of voltage-independent inactivation, presumed to involve the N-terminus (OI_1) and the outer pore region (OI_2), are coupled to channel opening. Closed state inactivation (CSI), is represented by the voltage-independent vertical transitions between the middle and lower row; voltage sensor activation is facilitated in inactivated channels (f = 0.3). During a strong depolarization channels ultimately accumulate in CI_4 in a process that has been referred to as preferential CSI. The modification to Model 2 of Bahring et al. is the addition of binding/unbinding of 4AP, represented by the vertical transitions between the upper and middle rows. Note that in this reaction scheme 4AP binding and CSI are explicitly mutually exclusive processes: inactivated channels do not bind 4AP and 4AP bound channels do not inactivate. Setting g to 1 causes voltage sensor movement to be the same in the top and middle rows, and it makes the affinity of

4AP for the closed states the same. The presumption that 4AP has no affinity for the OB state is based on the experimental observation that the unblocking rate during a step to 50 mV (see Fig. 3C) has no concentration dependence. See Table 2 for the details of the simulation parameters. As discussed in the text, two approaches were taken with respect to the gating transitions bounded by the dashed lines. It was found that the outcome of the simulation was the same whether the OB to O transition was assumed to be rate-limiting or if a stabilization of the pre-open closed state (C_4B) and destabilization of the OB state caused channel opening to be the rate-limiting step.

Tables

TABLE 1

A comparison of the experimental and simulated relative block values (mean ± SD) for the midpoint potential ($V_{1/2}$) and the slope factor (s) estimated by a least squares fit to a Boltzmann relationship (*Eqn*. 6)

	$V_{1/2}$ (mV)		s (mV)	
	Experimental	Simulated	Experimental	Simulated
Availability	-59.3 ± 0.3 (n = 9)	-61.6 ± 0.1	5.4 ± 0.2 (n = 9)	5.3 ± 0.2
Relative block, 2 mM 4AP	-56.4 ± 0.4 (n = 6)	-56.6 ± 0.2	4.2 ± 0.3 (n = 6)	4.1 ± 0.2
Relative block, 10 mM 4AP	-51.8 ± 0.2 (n = 10)	-50.8 ± 0.1	3.3 ± 0.4 (n = 10)	2.7 ± 0.1

JPET Fast Forward. Published on September 1, 2017 as DOI: 10.1124/jpet.117.243097
This article has not been copyedited and formatted. The final version may differ from this version.

TABLE 2

Parameter values for Scheme 4AP in which 4AP dissociation from open-bound channels is rate-limiting

Parameter	Value	Source
α	200 s^{-1} (0 mV)	(Bahring et al., 2001)
z_α	1.0	″
β	4 s^{-1} (0 mV)	″
z_β	1.58	″
k_{co}	400 s^{-1}	″
k_{oc}	1100 s^{-1}	″
k_{o_oi1}	300 s^{-1}	″
k_{oi1_o}	30 s^{-1}	″
k_{oi1_oi2}	30 s^{-1}	″
k_{oi2_oi1}	15 s^{-1}	″
k_{ci}	30 s^{-1}	″
f	0.3	″
k_{ic}	0.02 s^{-1}	see text
k_{on}	0.08 mM^{-1} s^{-1} (-80 mV)	Fig. 4C
L	[4AP]	
k_{off}	0.08 s^{-1} (-80 mV)	Fig. 4C
g	1	
k_{cb_ob}	= k_{co}	
k_{ob_cb}	= k_{oc}	
k_{ob_o}	100 s^{-1}	

JPET Fast Forward. Published on September 1, 2017 as DOI: 10.1124/jpet.117.243097
This article has not been copyedited and formatted. The final version may differ from this version.

Figures

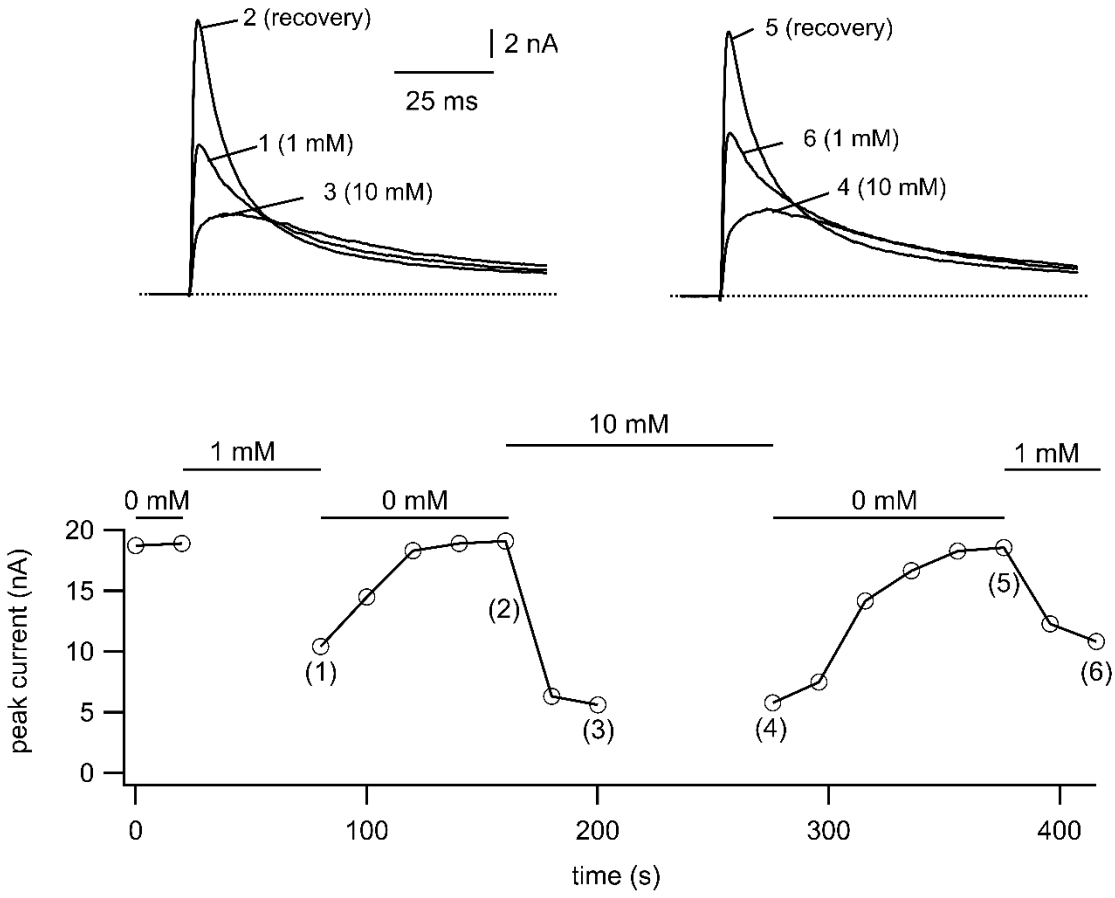

Figure 1

JPET Fast Forward. Published on September 1, 2017 as DOI: 10.1124/jpet.117.243097
This article has not been copyedited and formatted. The final version may differ from this version.

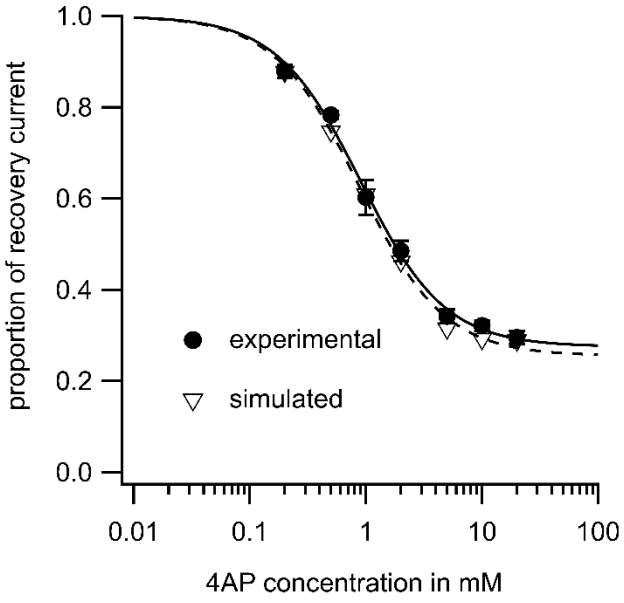

Figure 2

JPET Fast Forward. Published on September 1, 2017 as DOI: 10.1124/jpet.117.243097
This article has not been copyedited and formatted. The final version may differ from this version.

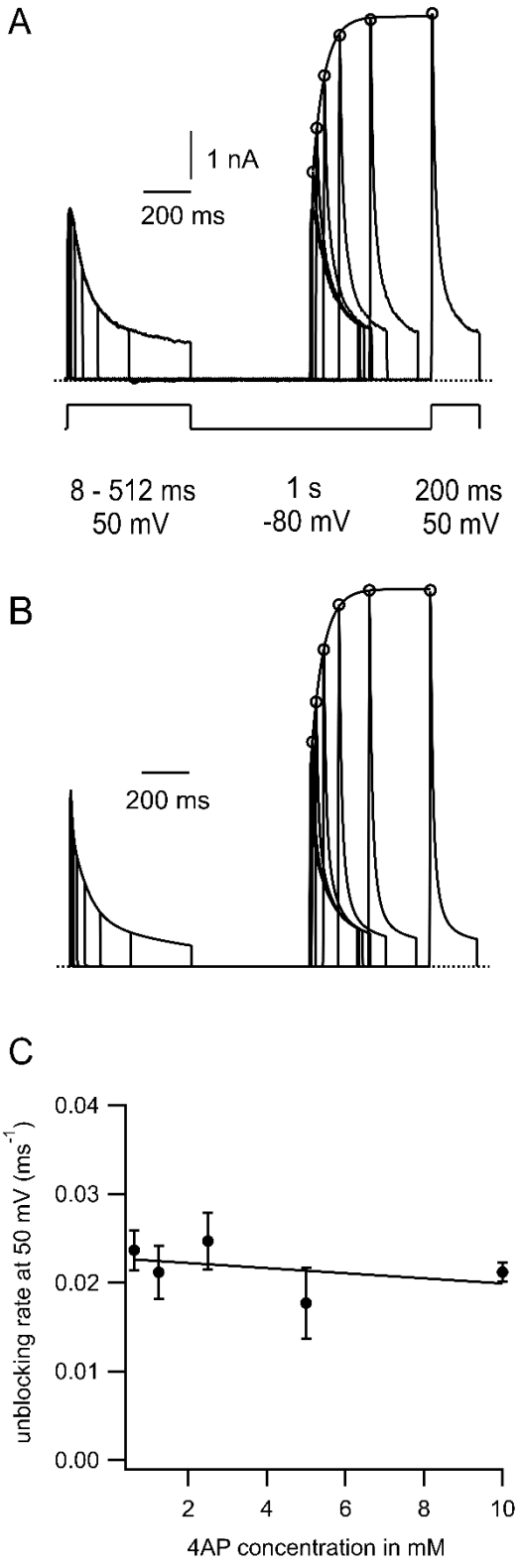

Figure 3

JPET Fast Forward. Published on September 1, 2017 as DOI: 10.1124/jpet.117.243097
This article has not been copyedited and formatted. The final version may differ from this version.

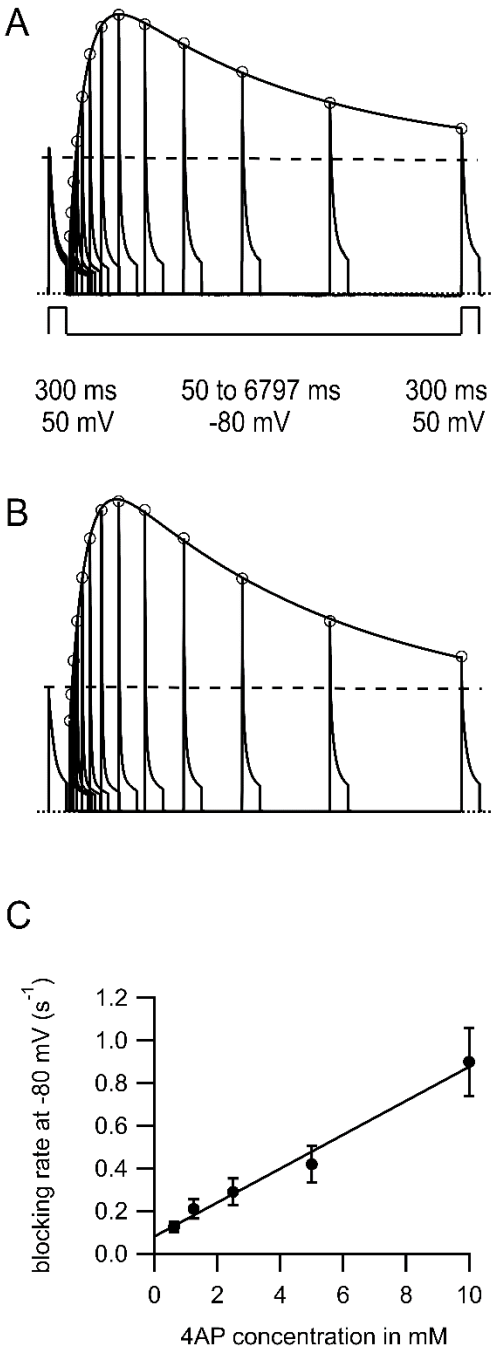

Figure 4

JPET Fast Forward. Published on September 1, 2017 as DOI: 10.1124/jpet.117.243097
This article has not been copyedited and formatted. The final version may differ from this version.

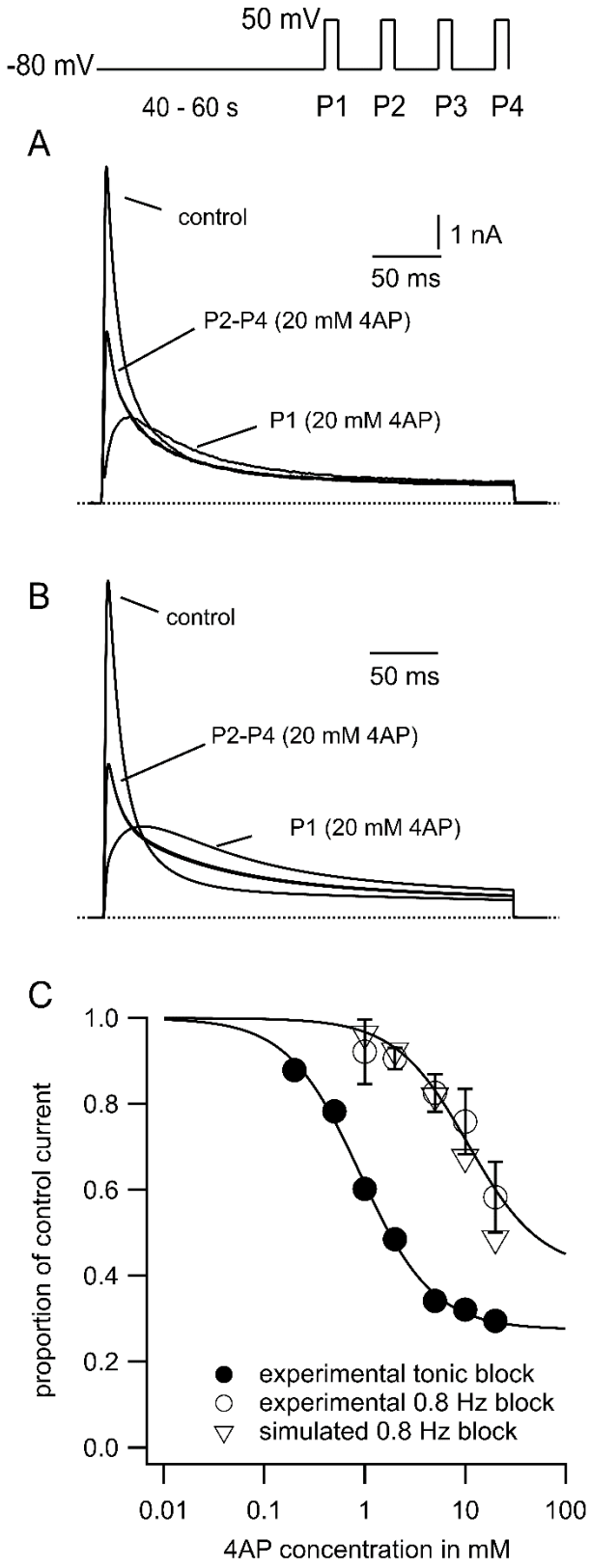

Figure 5

JPET Fast Forward. Published on September 1, 2017 as DOI: 10.1124/jpet.117.243097
This article has not been copyedited and formatted. The final version may differ from this version.

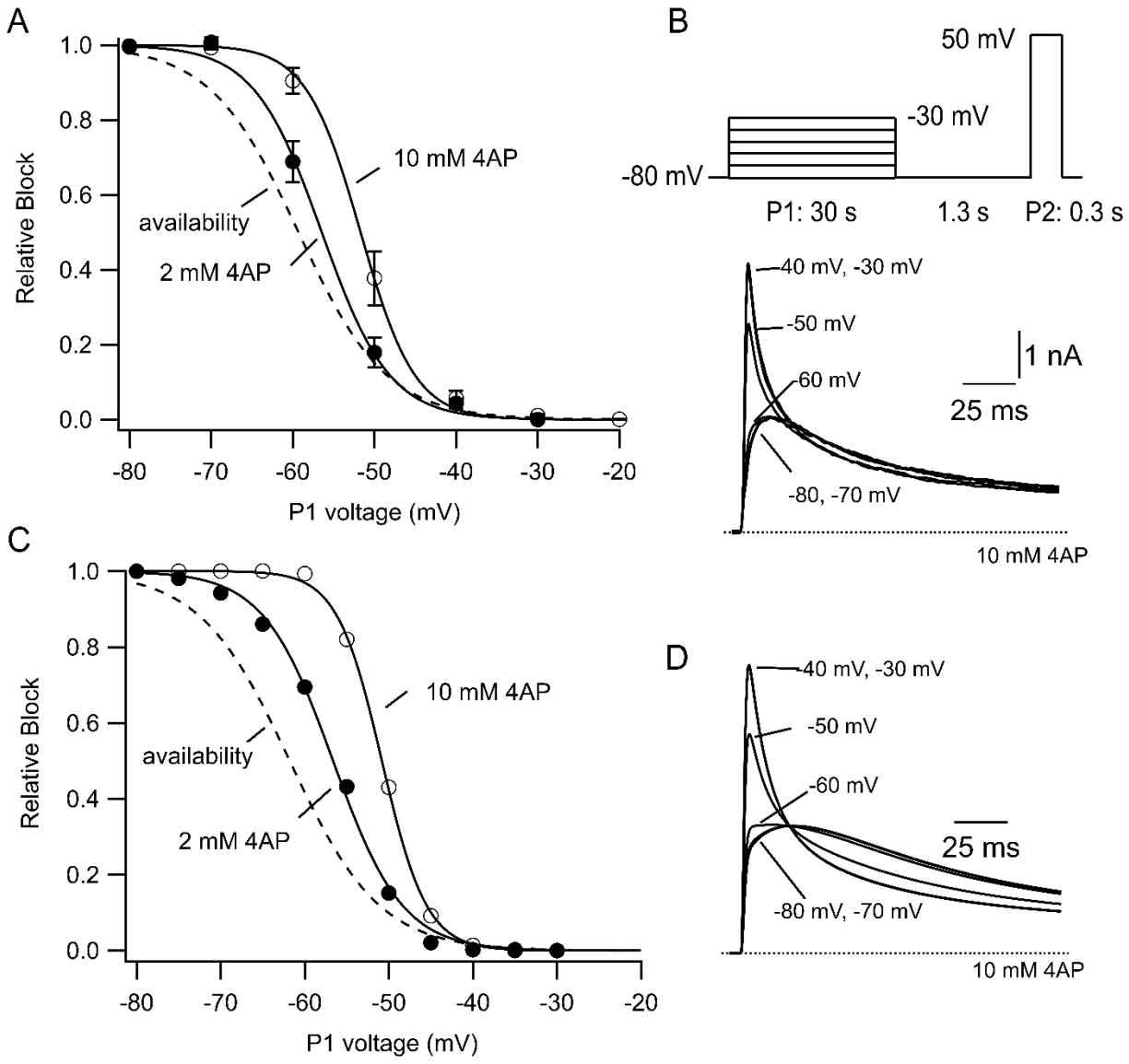

Figure 6

JPET Fast Forward. Published on September 1, 2017 as DOI: 10.1124/jpet.117.243097
This article has not been copyedited and formatted. The final version may differ from this version.

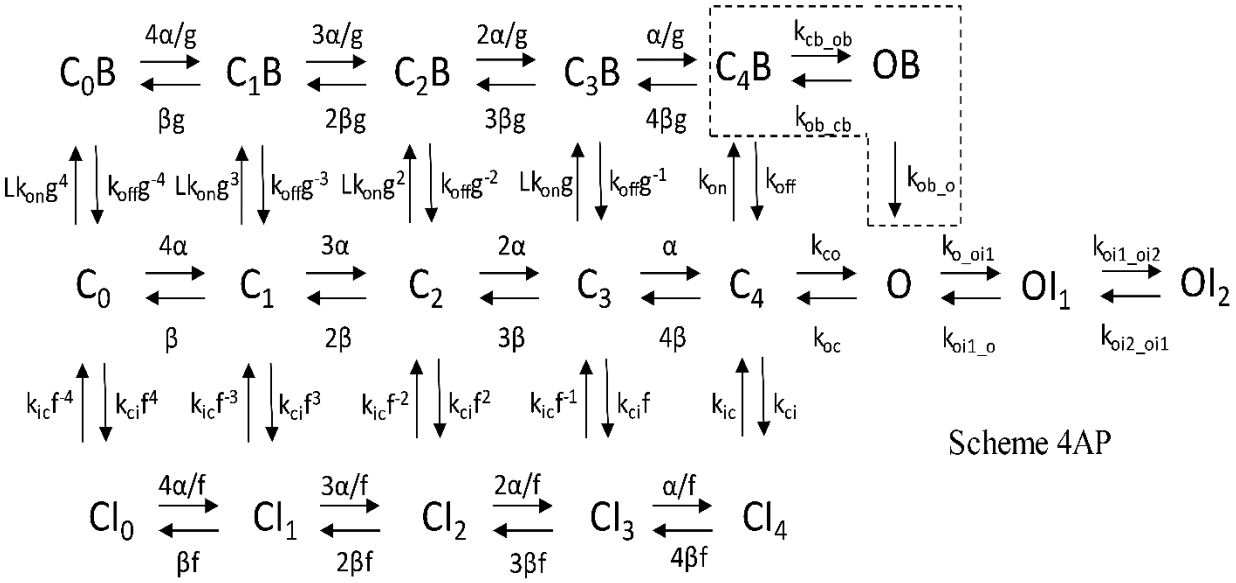

Scheme 4AP

Figure 7